Photo-electrical properties of single Cu-TCNQ nanowire

2014 Mater. Res. Express 1 045036

(http://iopscience.iop.org/2053-1591/1/4/045036)

Materials Research
Express

Photo-electrical properties of single Cu-TCNQ nanowire

Sun Sheng-sheng[1], Zhang Hua-qiang[2], Wang Qiang[1], Yu Jia-xin[1], Tian Zhao-shuo[2,1], Ren Xiu-yun[2,1], Zhao Jing[3], Liu Zhe[3] and Li Jun-jie[3]

[1] Department of Optics and Electronics Science, College of Science, Harbin Institue of Technology at Wei Hai, Wei Hai, 264209, People's Republic of China
[2] School of Information Technology and Electrical Engineering, Harbin Institute of Technology at Weihai, Weihai 264209, People's Republic of China
[3] Beijing National Laboratory for Condensed Matter Physics, Institute of Physics, Chinese Academy of Sciences, Beijing, 100190, People's Republic of China
E-mail: wq19750505@163.com and jjli@iphy.ac.cn

Received 18 September 2014, revised 24 October 2014
Accepted for publication 3 November 2014
Published 24 November 2014

Materials Research Express **1** (2014) 045036

doi:10.1088/2053-1591/1/4/045036

Abstract

In this letter, photo-electrical transport properties of individual Cu-TCNQ nanowire are studied. The electronic transport mechanism for single Cu-TCNQ nanowire well follows one-dimensional (1D) Mott's model in the temperature range from 80 to 300 K. The Cu-TCNQ nanowire shows photoconductivity at visible illumination, with much faster response time than recovery time. The thermionic emission (TE) and thermionic-field emission (TFE) models are employed to interpret the current versus voltage (*I*–*V*) plots, by considering fitted results for the reversely biased contact barriers. Our present work opens up potential applications of single Cu-TCNQ nanowire in organic photo-electric nanodevice.

Keywords: single Cu-TCNQ nanowire, 1D Mott's model, photoconductivity

1. Introduction

During the past decades, organic semiconductor devices such as light-emitting diodes, photovoltaic cells, chemical sensors and field-effect transistors have aroused considerable research interest because of their promising advantages such as low fabrication cost, high mechanical flexibility and versatility of the chemical structure [1–3]. As the elementary building blocks of nanoelectronic devices, individual nanowire has many advantages such as ultralow operation power, enhanced operation speed, etc. So far, single organic semiconductor nanowire

has attracted much attention for the design of nano-devices with unique photo-electrical characteristics.

Recent researches have drawn near the special concerns of stable organic semiconductor metal-tetracyanoquinodimethane (M-TCNQ) complexes, because they exhibit many extra-ordinary electrical and magnetic properties, and especially excellent resistive switching characteristics [4–6]. Therefore, it is considered to be the ideal choices for molecular electronics. Copper-TCNQ (Cu-TCNQ) is an organic charge transfer complex, which has two electrical phases: the high conductance phase (type I) and the low conductance phase (type II). The transition between these two phases is responsible for the electrical switching and memory effects [7, 8]. The optical/electrical properties of the Cu-TCNQ nanowires films (or self-assembled nanowires) have also attracted great interest recently [9], especially to mention the recent report of their photo-conductivity characteristics [1]. As we see, the optical/electrical properties of single nanowire are vital to understand nanoscale physics nature of Cu-TCNQ nano-devices, but it is rarely reported so far.

In this work, we have studied the photo-electronic properties of single Cu-TCNQ nanowire, which opens up potential applications of Cu-TCNQ nanowire in organic nanoelectronics and photoelectronics.

2. Experiments

Copper foil (99.99%) as substrate is cut into size of 2 cm × 4 cm, and immersed into the aqueous solution (33% wt) of nitric acid (HNO_3) for 5 min to obtain a polished surface, and then rinsed by de-ionized water before drying in a vacuum oven. TCNQ powder is spread into the Al_2O_3 carrier, and then covered with as-prepared copper foil. The temperature of constant temperature zone for the vacuum tubular CVD heater is preset at 200 °C, and argon gas is introduced to act as protective ambience. The ceramic carrier is pushed into the tubular heater, and the temperature is kept constant at 200 °C for 30 min. Evaporated TCNQ can react with Cu to form a product with deep-green color. At last, the carrier is pulled out at the tube edge to cool down naturally, and protective Ar gas is still introduced. After peeling off from copper foil, Cu-TCNQ nanowires films were then ultrasonically dispersed in ethanol to prepare well-isolated single Cu-TCNQ nanowire.

Scanning electron microscopy (SEM, FIB, DB235) and transmission electron microscopy (TEM, JEM-2010) are employed to characterize the morphologies and microstructures of as-formed Cu-TCNQ nanowires. Raman characterizations are carried out to study the chemical bonding states of as-formed products. By using the UV-Vis spectrophotometer (UV-1800, SHIMADZU), the UV/visible light absorption measurements are performed in air at room temperature. The Raman scattering properties are also characterized using micro-region Raman system (YJ-T64000). Just after obtaining well-isolated single Cu-TCNQ nanowire in ethanol solution, dipping onto substrate of SiO_2 (150 nm in thickness)/p^+-Si and nitrogen blow-drying are followed. Four-terminal (and two-probe) electrical contacts onto individual nonowire were fabricated using a standard procedure of electron beam lithography (EBL, Reith150), metallization, and lift-off. Magnetron-sputtering of 5 nm Cu film was followed by protective deposition of 100 nm Au film to form electrodes onto single Cu-TCNQ nanowire. Electrical transport measurements of single Cu-TCNQ nanowire are performed using the physical properties measurement system (PPMS, QUANTUM DESIGN) in the temperature range from

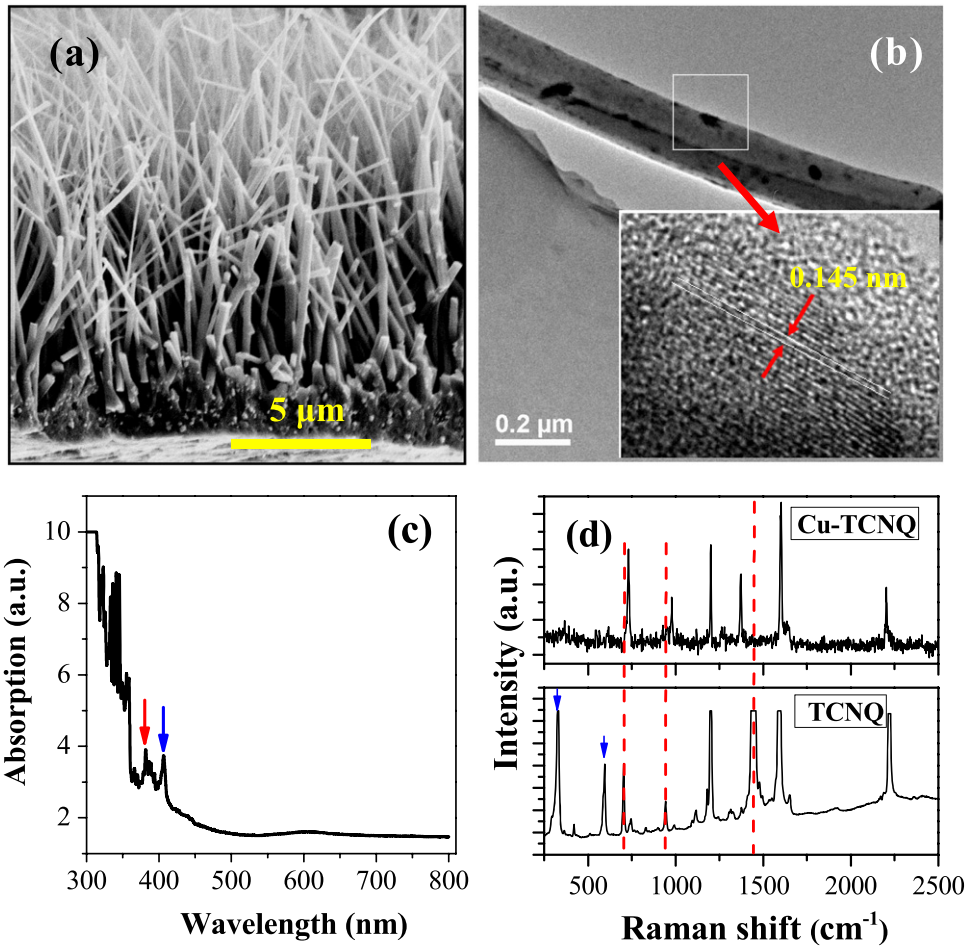

Figure 1. Microstructure characterizations of Cu-TCNQ nanowires. (a) SEM image of Cu-TCNQ nanowires. (b)TEM image of single Cu-TCNQ nanowire. (c) UV-Vis absorption spectra. (d) Raman spectra of Cu-TCNQ and TCNQ.

300 to 80 K at the driving voltage of 3 V. A Keithley 4200 electrical measurement system is employed to study the electrical transport properties of as-prepared single Cu-TCNQ nanowire. Under steady-state illumination of a standard solar simulator (AM1.5) powered by a 300 W xenon lamp, the visible light response of electrical current for single Cu-TCNQ nanowire in two-probe contact configuration was cyclically documented by controlling the cyclic on/off states of visible light through a single-chip microcomputer.

3. Results and discussion

The results for microstructure characterizations of Cu-TCNQ nanowires are shown in figure 1. Figure 1(a) shows the cross-sectional SEM image of Cu-TCNQ nanowires on Cu foil. Figure 1(b) shows the TEM image of single Cu-TCNQ nanowire with diameter of less than 200 nm, which is inset with the high resolution image, showing mainly amorphous structure and some crystallized parts with the lattices distance of 0.145 nm, the b axis length of neutral TCNQ [10]. Figure 1(c) shows the UV-Vis absorption spectrum of as-formed Cu-TCNQ nanowires,

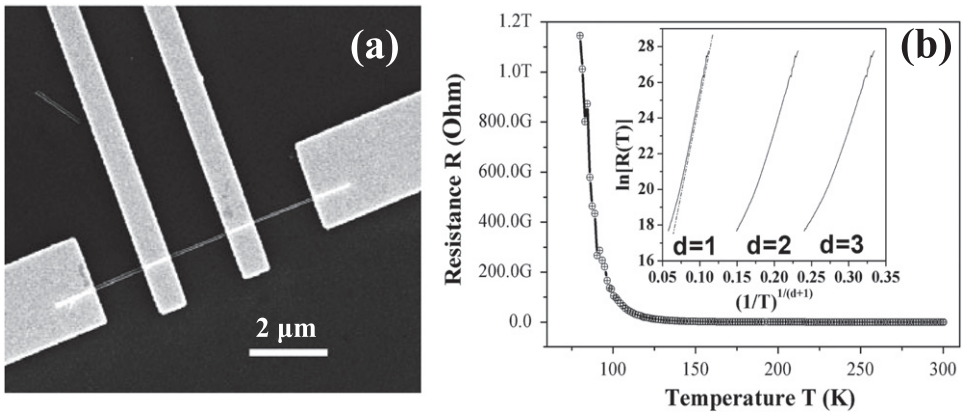

Figure 2. Electrical properties of single Cu-TCNQ nanowire studied by four-probe method. (a) SEM image, (b) *R–T* relation and theoretical fitting by using Mott transport mechanism.

Table 1. Raman peaks for TCNQ powder and Cu-TCNQ nanowires.

Peaks for TCNQ (cm^{-1})	335.4	598.2	707.6	946.1	1206.1	1447.7	1591.3	2221.9
Peaks for CuTCNQ (cm^{-1})	No	No	735.3	973.3	1204.2	1378.2	1603.9	2220.1
Peak shifts (cm^{-1})	No	No	27.7	27.2	1.9	−69.5	−12.6	−1.8

which shows two distinct peaks at 382.3 and 407.8 nm, respectively. These two peaks both originate from TCNQ radicals [11], which are also intrinsic absorption characteristics of Cu-TCNQ [1]. Figure 1(d) shows the Raman spectra of Cu-TCNQ and TCNQ, respectively, and some contrast values are shown in table 1. Raman spectroscopy has been proved to be extremely useful in fingerprinting M-TCNQ materials [12, 13], which is due to the significant shift to lower wave-numbers in the C–CN wing stretching mode at 1447.7 cm^{-1} (for neutral TCNQ) to 1378 cm^{-1} (for reduced state in Cu-TCNQ). Other blue or red Raman shifts are also recorded, while the definite origins need further study.

The electrical transport properties of single Cu-TCNQ nanowire in the temperature range of 80∼300 K are studied by four-probe method, which can reveal the intrinsic nature of nanowire by eliminating the contact resistance. Figure 2(a) shows the SEM picture of single Cu-TCNQ nanowire with four FIB-patterned micro-contacts. Figure 2(b) shows the resistance versus temperature (*R–T*) relation of this nanowire. The resistance *R* of this nanowire is changed from 45 MΩ (at 300 K) to 1.8 GΩ (at 150 K) and to 1.15 TΩ (at 80 K), which indicates the estimated conductivity σ is changed from $3.5\times10^{-2}\,s\cdot cm^{-1}$ to $1.4\times10^{-8}\,s\cdot cm^{-1}$. The inset curve in figure 2(b) shows theoretically fitted curve $\ln[R(T)]$ versus $(1/T)^{1/(d+1)}$ by using Mott transport mechanism, which exhibits best linearity by setting $d=1$.

A general Mott's description for resistance $R(T)$ of non-crystalline nanowire is given by [14, 15]

$$R(T) = R_0 \exp\left[\left(\frac{T_0}{T}\right)^{\frac{1}{d+1}}\right], \tag{1}$$

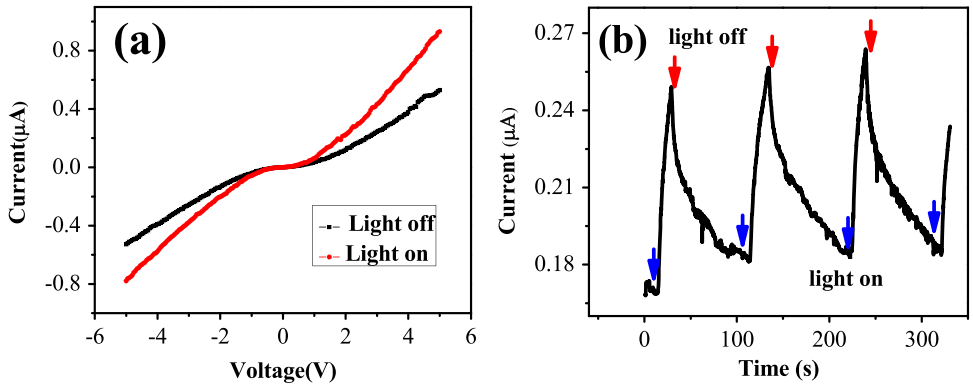

Figure 3. Visible light sensing properties of single Cu-TCNQ nanowire. (a) Current versus voltage (*I*–*V*) plots with light on and off, (b) current versus times (*I*–*t*) plots at cyclic illumination.

where R_0 is a material parameter, temperature-independent T_0 is a temperature scale defined by electronic states density $N(E_F)$ at the Fermi level E_F, and T is the working temperature. d is the dimension index for Mott transport mechanism, and $d = 1$ can well fit the one-dimensional transport mechanism for single Cu-TCNQ nanowire. As shown above, the conductivity σ of this nanowire is changed from $3.5 \times 10^{-2}\ \cdot^{-1}$ (80 K) to $1.4 \times 10^{-8}\ \cdot^{-1}$ (300 K). It thus indicates Cu-TCNQ nanowire may be a potential high-sensitivity temperature sensor in cryogenic environment, which may be more convenient than the fiber Bragg grating cryogenic temperature sensors [16].

Figure 3 shows visible light sensing properties of single Cu-TCNQ nanowire at the illumination of standard solar simulator. Figure 3(a) shows current versus voltage (*I*–*V*) plots with light on and off, which indicates the current is enhanced at visible light illumination. The contacts between semiconductor nanowire and metal leads can be in either high or low resistance states depending on the Fermi levels alignments and specific natures of interfaces between the metal and semiconductor nanowire. Thus, the non-rectifying electrical transport properties indicate that the two contact barriers for individual nanodevice may be rather similar. Figure 3(b) shows current versus times (*I*–*t*) plots at cyclic illumination with constant applied voltage of 2.5 V. For a specific illumination cycle of 100 s, the current is quickly increased from 0.18 to 0.26 μA with a duration of 17 s for the 'on' state, and it is rather slowly decreased back to 0.18 μA with a duration of 83 s for the 'off' state.

For the M-S-M back-to-back double contacts structure, the applied voltage is shared between the forward contact, the reverse contact, and the spread resistance of the semiconductor nanowire, that is, $V = V_{rev} + V_{for} + V_R$ [17]. But the voltage drop on the reverse contact is the dominant one, particularly for relatively small bias voltage, so $V \approx V_{rev}$. Here, V_{rev} is the voltage drop on the reverse barrier, V_{for} is the voltage drop on the forward barrier, and V_R is the voltage drop on the body of Cu-TCNQ nanowire.

The thermionic emission theory is generally employed for discussing the transport properties of M-S-M microelectronic devices, which assumes that the reverse current of an ideal Schottky junction should saturate at a very low and negligible value. As an electronic nano-system is considered, the measured current is typically of the order of tens of nA which is comparable to that of the reverse or leakage current in a Schottky diode. The tunneling current is therefore not negligible, and even becomes the dominating mechanism under large enough

reverse bias [18]. As a result, the thermionic-field emission (TFE) model is used to acceptably interpret the experimental transport results of many nano-devices. Following the TE model, the *I*–*V* relation can be expressed as [17]

$$I_{\mathrm{TE}} = I_{\mathrm{S}}\left[\exp\left(\frac{qV}{nkT}\right) - 1\right]. \tag{2}$$

Saturation current I_{S}, barrier height φ_b and electric field E can be expressed respectively as

$$I_{\mathrm{S}} = SA^{**}T^2\exp\left(-\frac{q\varphi_b}{kT}\right), \tag{3}$$

$$\varphi_b = \varphi_0 - \sqrt{qE/4\pi\varepsilon\varepsilon_0}, \tag{4}$$

$$E = \sqrt{\frac{2qN_D}{\varepsilon\varepsilon_0}\left(V + V_{\mathrm{bi}} - \frac{kT}{q}\right)}. \tag{5}$$

Here, $\left(V_{\mathrm{bi}} - \frac{kT}{q}\right)$ is the built-in potential, n is the ideality factor for M-S diode. When the contact barrier is reversely biased for the TE model, a reasonable relation $\ln(I_{\mathrm{TE}}) \propto \ln(I_{\mathrm{S}}) \propto V^{0.25}$ should be followed.

Following the TFE model, the *I*–*V* relation for the reversely biased barrier can be expressed as [17]

$$\begin{aligned} I_{\mathrm{TFE}} &= \frac{SA^{**}T\sqrt{\pi E_{00}}}{k}\sqrt{q\left[\frac{\varphi_b}{\cos\,\mathrm{h}^2\left(E_{00}/kT\right)} + V\right]} \\ &\quad\times\exp\left[q\left(\frac{V}{kT} - \frac{V+\varphi_b}{E_0}\right)\right] \\ &= SI_0\exp\left[qV\left(\frac{1}{kT} - \frac{1}{E_0}\right)\right], \end{aligned} \tag{6}$$

Where $E_0 = E_{00}\coth(E_{00}/kT)$, $E_{00} = \frac{hq}{4\pi}\sqrt{\frac{N_D}{\varepsilon\varepsilon_0 m^*}}$, and I_0 is a combined parameter. At reverse bias for the TE model, the current through the barrier should follow the relation $\ln\left(I_{\mathrm{TFE}}\right) \propto V$ on condition that the applied voltage V is not so large. If V is large enough, the relation $\ln\left(I_{\mathrm{TFE}}/V^{0.5}\right) \propto V$ should be checked [19].

Following the above TE and TFE formulas, theoretical fitting of experimental *I*–*V* plots with light on and off are performed. As can be seen from figure 4(a), the fitted results following $\ln(I_{\mathrm{TE}}) \propto \ln(I_{\mathrm{S}}) \propto V^{0.25}$ for the TE model are shown, which shows better linearity at low bias. As seen from figure 4(b), the fitted results following $\ln\left(I_{\mathrm{TFE}}\right) \propto V$ for the TFE model are shown, which shows better linearity at high bias. In figure 4(c), the fitted results following $\ln\left(I_{\mathrm{TFE}}/V^{0.5}\right) \propto V$ for the TFE model are shown, which shows no good linearity for all scanning bias. Combining the above analysis, it can be concluded that TE model works for low bias region, while TFE model works for high bias region. The modulation of I by applying bias V is not due to the modulation of carrier concentration in the nanowire body on condition that the reverse contact barrier dominates the electronic transport. As can be seen quantum-

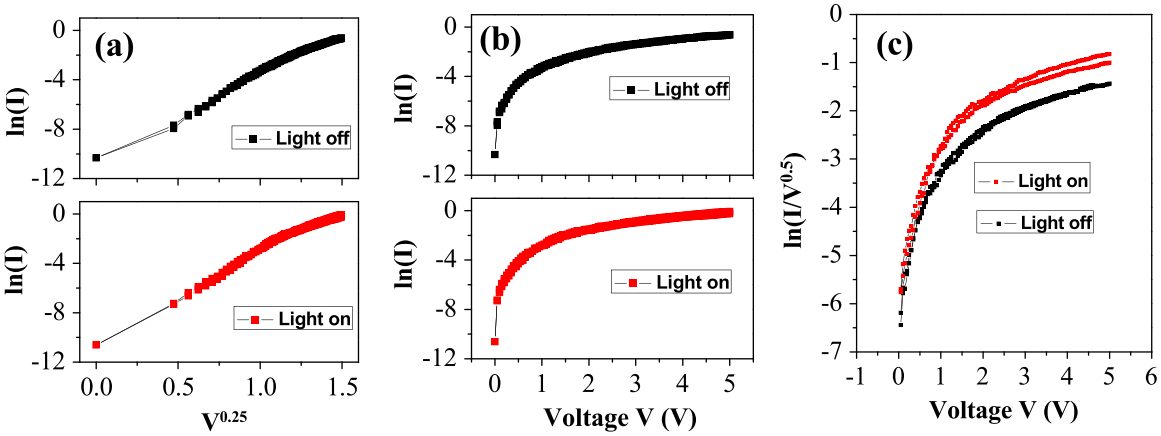

Figure 4. Theoretical fitting of experimental *I–V* plots with light on and off. (a) the fitted results following $\ln(I_{TE}) \propto \ln(I_S) \propto V^{0.25}$ for the TE model. (b) the fitted results following $\ln\left(I_{\mathrm{TFE}}\right) \propto V$ for the TFE model. (c) the fitted results following $\ln\left(I_{\mathrm{TFE}}/V^{0.5}\right) \propto V$ for the TFE model.

mechanically, the width of contact barrier can be effectively modulated at high bias *V*, by the shift of Fermi level in the high-resistance contact regions. This may be the applicable mechanism for the transition from TE model to TFE model at increasing applied voltage.

Intrinsically speaking, the photo-electrical properties of organic semiconductor are determined by the photo-modulated density of carriers and excitons. Because the high-resistant contact regions in as-fabricated CuTCNQ nano-unit dominate the total electrical resistance, the electronic origin of photo-conductivity to visible illumination is due to the photo-modulation of interfacial states in the contact regions. Incident photons will pump carriers from HOMO states to LUMO or inter-band sates, which will lower the transport barrier height. As a result, 'on' and 'off' states of transport current will be controlled by light illumination.

4. Conclusion

To summarize, single Cu-TCNQ nanowire nanodevices with ultra-high resistance-temperature response are fabricated, and the photo-electrical properties are studied. The Cu-TCNQ nanowire shows photoconductivity at visible illumination, with much faster response time than recovery time. The thermionic-field emission and thermionic emission models are employed to interpret the electronic transport properties as reflected from *I–V* plots, by considering the electronic tunneling effect at the different contact barriers at reverse bias. Our present studies of single metal tetracyanoquinodimethane nanowire pave the way for further study of its applications in nano-electronic science, and also illustrate a promising scheme for design of high-sensitivity temperature sensor in cryogenic environment by using single Cu-TCNQ nanowire.

Acknowledgments

This work was financially supported by the National Natural Science Foundation of China (NSFC) (Grand No. 11274082, 41306092, 91023041 and 11174362), and Shandong Excellent Young Scientist Research Award Fund Project (Grand No. BS2011CL002). Ren Xiuyun is also

thankful to the financial support of Natural Science Foundation of Shandong province (Grand No. ZR2013DQ026). Special thanks are given to the Fundamental Research Funds for the Central Universities (Grant No. HIT. BRET. 2010014) and the Knowledge Innovation Project of CAS (Grand No. KJCX2-EW-W02).

References

[1] Basori R, Das K, Kumar P, Narayan K S and Raychaudhuri A K 2013 *Appl. Phys. Lett.* **102** 061111
[2] Yang Y S, Yasuda T, Kakizoe H, Mieno H, Kino H, Tateyama Y and Adachi C 2013 *Chem. Commun.* **49** 6483
[3] Luber E J and Buriak J M 2013 *ACS Nano* **7** 4708
[4] Liu Y L, Jiang L, Dong H L, Tang Z Y and Hu W P 2011 *Small* **7** 1412
[5] Ouyang C B, Guo Y B, Liu H B, Zhao Y J, Li G X, Li Y J, Song Y L and Li Y L 2009 *J. Phys. Chem.* B **113** 7044
[6] Deleruyelle D, Muller C, Amouroux J and Muller R 2010 *Appl. Phys. Lett.* **96** 263504
[7] Heintz R A, Zhao H, Ouyang X, Grandinetti G, Cowen J and Dunbar K R 1999 *Inorg. Chem.* **38** 144
[8] Potember R S, Poehler T O and Cowan D O 1979 *Appl. Phys. Lett.* **34** 405
[9] Zhou Z, Xiao K, Jin R, Mandrus D, Tao J, Geohegan D B and Pennycook S 2007 *Appl. Phys. Lett.* **90** 193115
[10] Ballester L, Gutierrez A, Perpinan M F and Azcondo M T 1999 *Coordination Chem. Rev.* **190–192** 447
[11] Hiraishi K, Masuhara A, Yokoyama T, Kasai H, Nakanishi H and Oikawa H 2009 *J. Cryst. Growth* **311** 948
[12] Mahajan M, Bhargava K S and Anthony P 2013 *RSC Adv.* **3** 4440
[13] Zhao C, MacFarlane D R and Bond A M 2009 *J. Am. Chem. Soc.* **131** 16195
[14] Ma Y J, Zhou F, Lu L and Zhang Z 2004 *Solid State Commun.* **130** 313
[15] Wang Q, Li J J and Gu C Z 2012 *J. Phys. Chem.* C **116** 16864
[16] Guo Z, Feng J and Wang H 2012 *Cryogenics* **52** 457
[17] Antonakakis N S, Sarantopoulou E, Kollia Z, Samard Z, Kobe S and Cefalas A C 2012 *J. Appl. Phys.* **112** 094301
[18] Appenzeller J, Radosavljevic M, Knoch J and Avouris P 2004 *Phys. Rev. Lett.* **92** 048301
[19] Liao M, Wang X, Teraji T, Koizumi S and Koide Y 2010 *Phys. Rev.* B **81** 033304